

UNCLASSIFIED

AD NUMBER
AD217169
NEW LIMITATION CHANGE
TO Approved for public release, distribution unlimited
FROM Distribution authorized to DoD only; Administrative/Operational Use; Apr 1959. Other requests shall be referred to Commanding Officer, Ordnance Tank Automotive Command, Warren, MI.
AUTHORITY
USATAC Notice, 8 May 1970

THIS PAGE IS UNCLASSIFIED

AD 217 169

20020814272

9

Report No. _____

LL 63

Division of Engineering
BROWN UNIVERSITY
PROVIDENCE, R. I.

THE MECHANICS OF THE TRIAXIAL TEST FOR SOILS

by

R. M. HAYTHORNTHWAITE

**TECHNICAL LIBRARY
REFERENCE COPY**

U. S. Army Ordnance Corps
Ordnance Tank-Automotive Command
Contract DA-19-020-ORD-4566
Project: TBL-0007, Boston O. D.
Supervised by Detroit Arsenal
Tech. Rept. No. 1 April 1959

DA-4566/1

20020814272



AD 217 169

TABLE OF CONTENTS

	Page No.
Abstract.	1
Introduction.	2
The triaxial test.	2
The Coulomb yield criterion.	4
Stable plastic flow.	5
Limiting Equilibrium States	7
Failure with axial compression	7
Failure with axial extension	8
Plastic Solution for Plane Strain	10
Extent of the deformable region.	10
Dilatation	11
Plastic Solutions for Axial Symmetry.	12
Failure with axial compression	12
Failure with axial extension	14
Other solutions.	14
Experimental Evidence	16
Bibliography.	20
Appendix.	22
Table I	23
Table II.	24
Figures	
Distribution List	

THE MECHANICS OF THE TRIAXIAL TEST FOR SOILS*

R. M. HAYTHORNTHWAITE**

Abstract

Stress distributions at failure are not uniquely defined in terms of equilibrium and a failure criterion such as the Coulomb law which is commonly used for soils. This fact is illustrated in the paper by constructing alternative, non-uniform stress distributions for the triaxial test which lead to different apparent angles of friction. A suitable flow rule is introduced and complete solutions are obtained in which the external pressures causing failure are uniquely defined. Several alternative velocity fields are developed and the extent of the deformable zone is established. The analysis is used to discuss the significance of tests on sand where the specimens are caused to fail with axial extension rather than with the more conventional axial compression.

* This paper reports work sponsored by the Land Locomotion Research Branch, Ordnance Tank-Automotive Command, Detroit Arsenal, under Contract DA-19-020-ORD-4566.

** Associate Professor, Division of Engineering, Brown University, Providence 12, R. I.

Introduction

It is customary to base both the analysis of the stability of soil masses and the interpretation of soil tests upon the Coulomb theory of internal friction. This theory provides what in the terminology of plasticity theory is called a yield or failure surface and, together with the equilibrium conditions, it enables the failure loads to be computed whenever the problem is statically determinate. Other problems which are not intrinsically so can be rendered statically determinate by invoking the hypothesis of Haar and v.Kármán^[1], which asserts that the intermediate principal stress is equal to either the largest or the smallest principal stress. This hypothesis is particularly useful in axially symmetric problems.

The conventional approach outlined above suffers from the drawback that the solutions so obtained are not necessarily unique. To ensure uniqueness, a stress-strain relation of a particular type is required and the establishment of such a relation, if it exists, is one of the most important of the unsolved problems of soil mechanics.

This paper is concerned with an examination of the so-called triaxial test in the light of a particular stress-strain relation which would ensure both stability and uniqueness of the stresses if its validity could once be established by means of tests. The analysis is used to discuss the significance of tests on sand in which the specimens are caused to fail with axial extension rather than with the more usual axial compression.

The triaxial test. A detailed account of the triaxial test has been presented by Bishop and Henkel^[2] in a recent monograph. The essentials of the device are indicated in Fig. 1. A cylindrical specimen of soil is enclosed within a rubber membrane and mounted between stiff end plattens. Hydrostatic pressure is applied by means of an enveloping fluid, which is isolated from the specimen by a rubber membrane, and an extra axial thrust or pull can be exerted on the end plattens.

During a test, the relative displacement of the end plattens is observed, and sometimes the change in volume of the specimen and its change in diameter at a particular height are also observed. Testing proceeds by varying the axial load or the lateral pressure or, quite commonly, by imposing axial displacement of a platten and observing the resultant axial loads.

This apparatus now occupies a central position among the devices used to measure the strength of soils. It appears to have developed from a machine designed at the Prussian Waterways Experimental Station for the purpose of studying the consolidation of clays under conditions of negligible side friction^[3]. In this first apparatus the surrounding liquid was entirely confined, and temperatures and leakage had to be closely controlled to obtain consistent results. Several investigators recognized that the apparatus could be used to measure the ratio of the axial and lateral pressures both prior to and at failure, the first results being apparently those published by Stanton and Hveem^[4] in 1934. Positive control over the lateral pressure was developed independently by Rendulic^[5] working in Berlin, and by Housel^[6] at the University of Michigan.

Throughout the literature, it is assumed that a homogeneous state of stress is produced in the triaxial soil specimen. This point of view appears to have been taken over from the earlier studies of rocks by von Kármán and others and does not appear to have been questioned since that time. Strictly speaking, however, the problem posed by the test situation is statically indeterminate because only the total thrust on the end plattens, not the pressure distribution, is given as a boundary condition. Even allowing circular symmetry and similarity of conditions on every normal cross-section, there are still three unknown stresses σ_r , σ_θ and σ_z (see Fig. 2) and only two equilibrium equations:

$$\left. \begin{aligned} \frac{d\sigma_r}{dr} + \frac{\sigma_r - \sigma_\theta}{r} &= 0 \\ \frac{d\sigma_z}{dz} &= 0 \end{aligned} \right\} \quad (1)$$

If now σ_θ is equated arbitrarily to σ_r , σ_r is then constant by the first of (1) and the stress is homogeneous. This step has never been established a priori, but it has seemed reasonable in view of its correctness in the elastic range (at sections remote from the ends of the specimen). Moreover, some such assumption has been necessary before information about yield could be extracted from the test.

The Coulomb yield criterion. The weight of evidence from the triaxial test supports the friction criterion of Coulomb^[7], although minor departures are common. In this criterion the shear stress τ_0 causing slip on any plane is taken as the sum of a constant value, termed the cohesion, and an additional amount which is proportional to the normal pressure acting across the plane; thus

$$\tau_0 = c + \sigma \tan \phi \quad (2)$$

where c is the cohesion and σ the tensile stress across the plane. The angle ϕ is called the angle of friction of the material. This relationship follows a straight line in the $\sigma - \tau$ plane (Fig. 3), in which the representation of stress at a point due to Mohr^[8] can also be drawn. A stress state for which yield is incipient on some plane will be represented by a circle touching the failure line, such as that shown in the Figure. From the geometry of the triangle ABC, $(\sigma_3 - \sigma_1)/2 = [c \cot \phi + (\sigma_1 + \sigma_3)/2] \sin \phi$ where σ_1, σ_3 are principal stresses; hence after rearrangement

$$\sigma_1 = \sigma_3 \tan^2 \left(\frac{\pi}{4} + \frac{\phi}{2} \right) - 2c \tan \left(\frac{\pi}{4} + \frac{\phi}{2} \right). \quad (3)$$

It is a property of the Mohr circle that the angle subtended at B, Fig. 3, represents twice the angle of inclination of the plane on which the corresponding stresses act. Thus the critical condition represented by point C in Fig. 3 occurs on a plane the normal of which subtends an angle $(\frac{\pi}{4} + \frac{\phi}{2})$ with the normal to the plane on which σ_1 acts.

When the stresses in the triaxial specimen are assumed to be homogeneous, the lateral and axial pressures can be related at once through (3). It will be shown in the section on Limiting Equilibrium States that this solution is not unique.

Stable plastic flow. Lack of uniqueness can be resolved by introducing a stress-strain relation. It is not known whether a stress-strain relation exists for any particular soil: the purpose here is to make an initial assumption and then to examine the consequences, with a view to obtaining predictions that can be compared with experiments.

We shall assume an isotropic, stable soil which yields at stress combinations that are constant and not a function of the strains or of the stress history. This is the specification for a so-called 'ideally plastic' material. By a stable material is meant one from which work cannot be extracted in any loading program, and it follows from this definition^[9] that the yield surface of the material is convex when drawn in a space with the stress components as the axes. Also any plastic strain increment vector superimposed on the stress space with corresponding axes matching will lie in the direction of the outwards-drawn normal to the yield surface. If the yield surface has corners, the vector may lie between adjacent normals.

When the yield surface has a continuously turning tangent, the stresses in a deforming body are uniquely defined^[18]. If it contains flats, there may be some latitude, although the choice may often be restricted by the requirements of equilibrium^[19]. For a body with specified surface velocities which are uniform, as in the case of the triaxial specimen deforming between rigid plattens, it may be shown that the external tractions are unique despite the ambiguity in the internal stressing (see the Appendix).

The nature of the ideally plastic material which follows the Coulomb yield criterion has been investigated by Shield^[10] and certain results are

quoted here for reference.

Figure 4 shows the intersection of the yield surface (3) with a plane $\sigma_b = \text{const.}$, where σ_b is one of the principal stresses (not necessarily the intermediate principal stress). The regions corresponding to various orderings of σ_a , σ_b and σ_c are indicated. The strain rate vectors will lie in the directions of the outward drawn normals to the sides of the cross-section shown provided the components are related in the manner indicated in Table I. In this Table, the values $\lambda_1, \lambda_2, \dots, \lambda_6$ are constants and $N = \tan\left(\frac{\pi}{4} + \frac{\varphi}{2}\right)$.

In each line of Table I, the sum of the strain rates is proportional to $N^2 - 1$ and the sum of the absolute values to $N^2 + 1$; hence

$$\varepsilon_a + \varepsilon_b + \varepsilon_c = (|\varepsilon_a| + |\varepsilon_b| + |\varepsilon_c|) \sin \varphi \geq 0.$$

At least one of the three components is positive and at least one negative.

Denote the positive component by ε_α and the negative by ε_γ . When the third component ε_β is positive

$$\varepsilon_\alpha + \varepsilon_\beta + \varepsilon_\gamma \tan^2\left(\frac{\pi}{4} + \frac{\varphi}{2}\right) = 0 \quad (4)$$

and when ε_β is negative,

$$\varepsilon_\alpha \tan^2\left(\frac{\pi}{4} - \frac{\varphi}{2}\right) + \varepsilon_\beta + \varepsilon_\gamma = 0. \quad (5)$$

At the apex x , the rate of energy dissipation $D = \sum \sigma_i \varepsilon_i$ is

$$D = c \cot \varphi (\varepsilon_1 + \varepsilon_2 + \varepsilon_3) = c \delta \cot \varphi \quad (6)$$

where δ is the dilatation rate per unit volume. Expression (6) also applies at all other points on the pyramid because the projection of the stresses in directions normal to the sides is always the same.

Using the ideally plastic material described above, it is possible to obtain a unique solution for the applied pressures in the triaxial test. This will be done below, but first the lack of uniqueness of the so-called 'limiting

equilibrium states' will be demonstrated by exhibiting alternative solutions.

Limiting Equilibrium States

A limiting equilibrium state will be defined as an equilibrium stress distribution in which the soil reaches failure at a sufficient number of points for slip to appear possible. In the case of the triaxial test, limiting equilibrium states can be based on a homogeneous stress distribution, but there are alternatives, based on non-homogeneous distributions, which meet the hypothesis of Haar and v. Karman and a still wider class of solutions that does not.

For the purposes of illustration a general class of solutions is developed below in which the principal stresses remain in constant ratio at all points in the specimen, although the stress level may vary from point to point in the radial direction.

Failure with axial compression. Shortening of the specimen will occur when the average axial pressure $\bar{q} = -\sigma_z$ exceeds the lateral pressure $p = -[\sigma_r]_{r=a}$. Assuming $\sigma_r > \sigma_z$, (3) becomes

$$\sigma_r = \sigma_z N^2 - 2cN \quad (7)$$

where $N = \tan\left(\frac{\pi}{4} + \frac{\phi}{2}\right)$. The position of the intermediate principal stress σ_θ can be expressed by the coefficient k where

$$\sigma_\theta = k \sigma_r + (1-k) \sigma_z \quad (8)$$

and $1 \geq k \geq 0$. Substituting (7) and (8) in the first of (1), integrating and making use of the boundary condition $[\sigma_r]_{r=a} = -p$,

$$\sigma_r = c \cot \phi - (p + c \cot \phi) \left(\frac{r}{a}\right)^{(N^2-1)(k-1)} \quad (9)$$

and

$$\sigma_z = c \cot \phi - N^2 (p + c \cot \phi) \left(\frac{r}{a}\right)^{(N^2-1)(k-1)} \quad (10)$$

It is confirmed that $\sigma_r > \sigma_z$, because $N^2 > 1$. On integrating σ_z over the normal cross-section, the expression for the mean axial pressure \bar{q} becomes

$$\bar{q} = \frac{2 [N^2 p + (1+k)Nc]}{(1-k)N^2 + 1 + k} \quad (11)$$

Setting $k = 1$ ($\sigma_\theta = \sigma_r$), the stress distribution is homogeneous and (8) reduces to the well-known result

$$\bar{q} = p \tan^2\left(\frac{\pi}{4} + \frac{\phi}{2}\right) + 2c \tan\left(\frac{\pi}{4} + \frac{\phi}{2}\right) \quad (12)$$

while on setting $k = 0$ ($\sigma_\theta = \sigma_z$),

$$\bar{q} = (1 + \sin \phi) p + c \cos \phi \quad (13)$$

The stress states giving rise to (12) and (13) both meet the hypothesis of Haar and v. Kármán, in that the intermediate principal stress is in each case equal to one of the extreme stresses. In addition, any number of alternative expressions may be obtained from the stress distributions associated with other values of k .

Failure with axial extension. Analogous results can be obtained for the case where the lateral pressure p exceeds the average axial pressure and axial extension occurs during failure. In this case it is assumed that $\sigma_r < \sigma_z$ and (3) becomes

$$\sigma_z = \sigma_r N^2 - 2 cN \quad (14)$$

Integrating the first of (1) after substituting (14),

$$\sigma_r = c \cot \phi - (p + c \cot \phi) \left(\frac{r}{a}\right)^{\left(\frac{1}{N^2} - 1\right)(1-k)} \quad (15)$$

and

$$\sigma_z = c \cot \phi - \frac{1}{N^2} (p + c \cot \phi) \left(\frac{r}{a}\right)^{\left(\frac{1}{N^2} - 1\right)(1-k)} \quad (16)$$

Here $\frac{1}{N^2} < 1$, so $\sigma_r < \sigma_z$. On integration of (16) over the cross-section

$$\bar{q} = \frac{2 [p - (1+k)Nc]}{(1+k)N^2 + 1 - k} \quad (17)$$

When $k = 1 (\sigma_\theta = \sigma_r)$, (17) gives the usual formula for the homogeneous stress distributions:

$$\bar{q} = p \tan^2\left(\frac{\pi}{4} - \frac{\phi}{2}\right) - 2c \tan\left(\frac{\pi}{4} - \frac{\phi}{2}\right) \quad (18)$$

while on setting $k = 0 (\sigma_\theta = \sigma_z)$,

$$\bar{q} = (1 - \sin \phi)p - c \cos \phi \quad (19)$$

Again both (18) and (19) satisfy the hypothesis of Haar and v. Kármán, intermediate formulae being obtained by using other values of k .

The ranges of possible values of \bar{q} represented by (11) and (17) are illustrated in Figure 5 for the particular case $c = 1$ and $\phi = 20^\circ$.

In the case of axial compression, the usual formula (12), represented by the upper boundary of the shaded zone, gives the highest possible values of \bar{q} . Loading paths which start at a hydrostatic pressure state ($\bar{q} = p$) must cross a zone in which, according to limiting equilibrium theory, failure is possible with a non-uniform stress distribution.

In the above illustration of alternative stress states, it is assumed that the principal stresses are in constant ratio, although there is no obvious reason why this should be so. If the assumption is abandoned and k made a function of the radius, many other stress distributions all satisfying the yield condition and the boundary conditions become possible.

A choice between all these solutions can be made by introducing a stress-strain relation such as that described in the Introduction. The particular stress-strain relation which has been selected narrows the choice to the point where the external tractions become uniquely defined and a rational comparison with test data becomes possible. With the aid of this relation, several possible velocity fields will be found which are associated with the homogeneous stress state.

Plastic Solution for Plane Strain

Suppose a single plane slip band of width t forms across the width of the specimen (Fig. 6). For plane strain $\epsilon_2 = 0$ and ϵ_1, ϵ_3 are given by

$$\frac{1}{2}(\epsilon_x + \epsilon_y) + \frac{1}{2} \left\{ (\epsilon_x - \epsilon_y)^2 + \gamma_{xy}^2 \right\}^{\frac{1}{2}}$$

Substituting in either (4) or (5),

$$\epsilon_y = \gamma_{xy} \tan \phi \quad . \quad (20)$$

Thus the direction of motion of one side of the slip band relative to the other subtends an angle ϕ with the direction of the band. The corresponding velocity field is

$$\left. \begin{aligned} u_x &= \frac{yu_0 \tan \phi}{t} \\ u_y &= \frac{yu_0}{t} \end{aligned} \right\} \quad (21)$$

in the slip band ($t \geq y \geq 0$). Both in the case of axial compression (Fig. 6a) and of axial extension (Fig. 6b), velocity fields have now been found that are associated with the (7) and (14) respectively. The remainder of the specimen is not stressed above yield and the solution is complete.

Extent of the deformable region. The extent of the deformable region can now be found by using the theorem due to Bishop, Green and Hill^[11] which states that any region shown to be necessarily rigid for a particular stress field (by arguments based solely on the geometrical and other properties of that field) must be rigid in all complete solutions. The slip lines form the characteristics both for the stress [12] and the velocity equations, and they serve to isolate regions at the ends of the specimens (as indicated in Fig. 7) which are necessarily rigid because the velocity will be continuous across the surface of the plattens. Figure 7 can represent any diametral cross-section, so the necessarily rigid zones are conical.

Dilatation. The total dilatation can be computed from the strains (20) or directly from energy considerations. By adopting the latter method, the dilatation rate can be shown to be independent of the precise nature of the velocity field. It is most convenient to consider separately the action of the hydrostatic pressure p and the excess axial load P . Equating the work done by the external forces during unit axial compression to the internal energy dissipation computed from (6),

$$P - p \Delta = c \cot \phi \int \delta dv = c \Delta \cot \phi \quad (22)$$

where Δ is the dilatation of the entire specimen per unit axial compression.

In the case of failure by axial compression, (7) applies, and it can be rewritten

$$p = \frac{P}{\pi a^2(N^2-1)} - c \cot \phi \quad ; \quad (23)$$

hence, comparing (22) and (23),

$$\Delta = \pi a^2(N^2-1) \quad . \quad (24)$$

In the case of failure by axial extension, (14) applies, and it can be rewritten

$$p = \frac{P}{\pi a^2\left(\frac{1}{N^2}-1\right)} - c \cot \phi \quad ; \quad (25)$$

so in this case

$$\Delta = \pi a^2\left(\frac{1}{N^2} - 1\right) \quad (26)$$

The above plane strain solution establishes a possible velocity field for the homogeneous stress distribution (obtained by setting $\sigma_\theta = \sigma_r$) but, although it establishes unique external pressure values, it does not ensure uniqueness of the stress distribution, due to the presence of flats on the yield surface.

Plastic Solutions for Axial Symmetry

The analysis given below follows closely that given by Shield^[13] for the case of a metal ($\varphi = 0$).

Due to the assumption that the material remains isotropic, the principal directions of strain will coincide with the principal directions of stress; hence

$\gamma_{rz} = 0$, or, denoting the radial and axial velocities by u and w respectively,

$$\frac{\partial u}{\partial z} + \frac{\partial w}{\partial r} = 0 \quad (27)$$

Other strain components are

$$\epsilon_r = \frac{\partial u}{\partial r}; \quad \epsilon_\theta = \frac{u}{r}; \quad \epsilon_z = \frac{\partial w}{\partial z} \quad (28)$$

Now consider possible stress states, Fig. 4, for definiteness setting $\sigma_a = \sigma_r$,

$$\sigma_b = \sigma_\theta \quad \text{and} \quad \sigma_c = \sigma_z.$$

Failure with axial compression. In the case of failure by axial compression, $\sigma_r > \sigma_z$ and, when σ_θ is the intermediate principal stress, only state points on side AF, Fig. 4 need be considered. On side AF, except at A and at F, $\epsilon_\theta = 0$ by Table I, then $\epsilon_r = 0$ by (28) and $\epsilon_z = 0$ by (4) or (5); hence no solution is possible. Possible solutions are thus immediately restricted to the state points A and F.

At F ϵ_θ is positive from Table I, so (4) applies. Recalling (27) and writing (4) in terms of the velocity components by means of (28), two simultaneous partial differential equations for the velocities are obtained:

$$\left. \begin{aligned} \frac{\partial u}{\partial r} + \frac{u}{r} + \frac{\partial w}{\partial z} \tan^2 \left(\frac{\pi}{4} + \frac{\phi}{2} \right) &= 0 \\ \frac{\partial u}{\partial z} + \frac{\partial w}{\partial r} &= 0 \end{aligned} \right\} \quad (29)$$

Shield has solved these equations for the particular case $N=1$ and solutions for $N \neq 1$ can be found along exactly the same lines. A first deforming zone is shown in Figure 8a, which illustrates one half of the cross-section. Continuity of

velocity is assumed across OB so that $u = w = 0$ on OB except at o. Neither (29) nor the boundary conditions involve a fundamental length, so u and w will be functions of ψ only (see Fig. 8a), and (29) reduces to

$$\left. \begin{aligned} -u' \sin \psi + u \sec \psi + w \tan^2 \left(\frac{\pi}{4} + \frac{\phi}{2} \right) \cos \psi &= 0 \\ u' \cos \psi - w' \sin \psi &= 0 \end{aligned} \right\} \quad (30)$$

where the primes denote differentiation with respect to ψ . The dependent variables can be separated by the substitution $x = \tan \psi$, leading to the solution

$$\left. \begin{aligned} u &= \frac{2}{\pi} \sqrt{\tan^2 \left(\frac{\pi}{4} + \frac{\phi}{2} \right) - \tan^2 \psi} \\ w &= \frac{2}{\pi} \tan^{-1} \sqrt{\tan^2 \left(\frac{\pi}{4} + \frac{\phi}{2} \right) \cot^2 \psi - 1} \end{aligned} \right\} \quad (31)$$

where the inverse tangent lies between 0 and π . The strain rates are in the ratio

$$\epsilon_r : \epsilon_\theta : \epsilon_z = \tan^2 \psi : \tan^2 \left(\frac{\pi}{4} + \frac{\phi}{2} \right) - \tan^2 \psi : -1 \quad (32)$$

so it is confirmed that ϵ_r and ϵ_θ are positive when ϵ_z is negative. The angle ψ varies from zero to $\left(\frac{\pi}{4} + \frac{\phi}{2} \right)$ and the resulting velocity vectors cover the entire range of permissible directions at the point F, as indicated in Fig. 4. The velocity field can be associated with one and only one stress point, so that for the velocity field (31) the stresses are uniquely defined despite the presence of flats on the yield surface. As a consequence it is not necessary to investigate state point A as a possibility. (If this is done, it is found that the strains have incorrect signs.)

The total dilatation rate has been found previously by energy considerations; it can also be found by integrating the sum of the strain rates over the deforming region.

The nature of the deformation (31) is indicated in Figure 9a, which

shows the deformed shape of an initially square grid obtained by assuming the initial velocities are maintained for a finite deformation.

Failure with axial extension. In this case $\sigma_r < \sigma_z$ and failure states lie on side CD of Figure 4. Except at C and D, $\epsilon_\theta = 0$ by Table I, and no solution is possible. At C, ϵ_θ is negative, so (5) applies, which with (27) gives

$$\left. \begin{aligned} \frac{\partial u}{\partial r} + \frac{u}{r} + \frac{\partial w}{\partial z} \tan^2\left(\frac{\pi}{4} - \frac{\phi}{2}\right) &= 0 \\ \frac{\partial u}{\partial z} + \frac{\partial w}{\partial r} &= 0 \end{aligned} \right\} \quad (33)$$

Adopting the deforming region indicated in Figure 8c and proceeding exactly as in the axial compression case, the velocities are found to be

$$\begin{aligned} u &= -\frac{2}{\pi} \sqrt{\tan^2\left(\frac{\pi}{4} - \frac{\phi}{2}\right) - \tan^2 \psi} \\ w &= -\frac{2}{\pi} \tan^{-1} \sqrt{\tan^2\left(\frac{\pi}{4} - \frac{\phi}{2}\right) \cot^2 \psi - 1} \end{aligned} \quad (34)$$

where again the inverse tangent lies between 0 and π . The strain rates are in the ratio

$$\epsilon_r : \epsilon_\theta : \epsilon_z = -\tan^2 \psi : -\tan^2\left(\frac{\pi}{4} - \frac{\phi}{2}\right) + \tan^2 \psi : 1$$

which is consistent only with the state point C, Figure 4. Thus the homogeneous stress state is the only possible one with the velocities (34). The nature of the deformation is indicated in Figure 9b.

Other solutions. The above solution serves to identify the homogeneous stress state with an axially symmetric mode of deformation. That the mode considered is not unique is established by the alternative solution given below. This second field also follows closely a field used by Shield^[13] for the case of a metal ($\phi = 0$). The deforming region is indicated in Figure 8b, which shows half the cross-section. We shall consider only axial compression, for which the differential equations to be solved are (29). In the region OAB the field used is

$$\left. \begin{aligned} u &= \frac{r}{2a} \tan\left(\frac{\pi}{4} + \frac{\phi}{2}\right) \\ w &= -\frac{z}{a} \tan\left(\frac{\pi}{4} - \frac{\phi}{2}\right) \end{aligned} \right\} \quad (35)$$

which satisfies (29) and the boundary condition $w = 1$ on AB. The velocity across OA is proportional to the distance R from O, so it is assumed that in AOC the field is of the form

$$u = RF(\psi) ; \quad w = RG(\psi) \quad (36)$$

where F and G are functions of ψ only. The condition that the normal velocity across OA be continuous (OA is a slip direction for the stress field being considered) requires

$$F \tan\left(\frac{\pi}{4} + \frac{\phi}{2}\right) + G = \left[1 + \frac{1}{2}\tan^2\left(\frac{\pi}{4} + \frac{\phi}{2}\right)\right] / a \sqrt{\tan^2\left(\frac{\pi}{4} + \frac{\phi}{2}\right) + 1}$$

on OA and $F = G = 0$ on OC. Substitution of (35) in (29) gives

$$\left. \begin{aligned} F(\cos\psi + \sec\psi) - F'\sin\psi + G\tan^2\left(\frac{\pi}{4} + \frac{\phi}{2}\right)\sin\psi \\ + G'\tan^2\left(\frac{\pi}{4} + \frac{\phi}{2}\right)\cos\psi = 0 \\ F\sin\psi + F'\cos\psi + G\cos\psi - G'\sin\psi = 0 \end{aligned} \right\} \quad (37)$$

where the primes indicate differentiation with respect to ψ . The variables are separated after making the substitutions $F = A(\psi)\cos\psi$; $G = B(\psi)\sin\psi$ and the solution satisfying the boundary conditions on F and G is found to be

$$\begin{aligned} u=RF &= \frac{R \left[\tan^2\left(\frac{\pi}{4} + \frac{\phi}{2}\right)\cos\psi \tan^{-1} \sqrt{\tan^2\left(\frac{\pi}{4} + \frac{\phi}{2}\right)\cot^2\psi - 1} - \sin\psi \sqrt{\tan^2\left(\frac{\pi}{4} + \frac{\phi}{2}\right) - \tan^2\psi} \right]}{2\pi a \tan\left(\frac{\pi}{4} + \frac{\phi}{2}\right)} \\ w=RG &= \frac{R \left[\cos\psi \sqrt{\tan^2\left(\frac{\pi}{4} + \frac{\phi}{2}\right) - \tan^2\psi} - \sin\psi \tan^{-1} \sqrt{\tan^2\left(\frac{\pi}{4} + \frac{\phi}{2}\right)\cot^2\psi - 1} \right]}{\pi a \tan\left(\frac{\pi}{4} + \frac{\phi}{2}\right)} \end{aligned} \quad (38)$$

where the inverse tangent lies between 0 and π . The strain rates are in the ratio

$$\epsilon_r : \epsilon_\theta : \epsilon_z = 1 + \frac{\gamma \sqrt{1 - \gamma^2}}{\cos^{-1} \gamma} : 1 - \frac{\gamma \sqrt{1 - \gamma^2}}{\cos^{-1} \gamma} : -2 \tan^2\left(\frac{\pi}{4} - \frac{\phi}{2}\right)$$

where $\gamma = \tan\left(\frac{\pi}{4} + \frac{\phi}{2}\right) / \tan\psi$. This is consistent with point F on the yield surface, Figure 4.

All the solutions given above are associated with the homogeneous stress distribution, the axially symmetric modes being associated with that distribution and no other. While it cannot be proved that other stress distributions are impossible, in view of the flats on the yield surface, they appear highly unlikely. Moreover, their identification, if they exist, would serve no useful purpose because the present solutions give unique values for the external pressure ratio and the dilatation and serve to show that both plane strain and axially symmetric deformation modes do in fact exist for an ideally plastic material that fails according to the Coulomb yield criterion.

Experimental Evidence

The above analysis enables the triaxial test to be used to check the validity of the hypothesis of Haar and v. Kármán by a comparison of the results of extension and compression tests. The complete plastic solutions are of value in that greater significance is now placed upon the Haar and v. Kármán hypothesis, for its validity becomes a necessary (but not sufficient) condition for the soil to behave as an ideally plastic material.

Several series of tests on sands under extension have been described in the literature, and the results are summarized in Figure 10. The theoretical lines in this Figure were computed by means of (15) and (16) and represent the extremes of \bar{q}/p theoretically possible while σ_θ remains the intermediate principal stress and the ratio of the principal stresses is constant. The test results are plotted under the assumption that $\sigma_\theta = \sigma_r$ in the compression test. They lie in the expected zone, but there is a considerable discrepancy between the results obtained by Habib^[14], [15] in 1951 and 1953 and those obtained by Bishop and Eldin^[16] and by Kirkpatrick^[17] in 1953 and 1957 respectively. A series of tests was undertaken in an attempt to obtain more information, and these new results are also indicated in Figure 10.

The new series was run on a crushed quartz from Lantern Hill, Mystic, Conn., U.S.A. The quartz was almost pure, being of glass making quality. The fraction used in the tests was that retained on a No. 50 sieve (opening 297 microns) and passing a No. 45 sieve (opening 350 microns). The sand was placed dry by tamping in three layers, and was then saturated with water before testing. The mean relative density achieved by this process was 70%.

The detailed results are given in Table II and in Figure 11. Two methods of reaching the failure state were used -- varying the axial load and reducing the lateral pressure. In each case failure was deemed to have occurred when the modulus was reduced to 10 kg/cm^2 , in terms of whichever pressure was being varied. The direction of approach to the failure point is indicated in Figure 11 by a short line running out from each point. A mean line has been drawn through the compression test results, and the angle of friction computed from this line (35.6°) was used to compute the two theoretical lines shown for the extension test using (18) and (19). The experimental results for the extension tests fall in between the theoretical lines, the tests with failure by reducing the axial pressure showing some scatter and those with failure by reducing the lateral pressure very little. Typical points are also plotted in Figure 10 where they fall close to those established by Habib.

Rates of volume increase per unit axial compression are also given in Table II. These are the average values at failure. It should be noted that in series C and D the specimens were extending, so negative values of the dilatation per unit axial compression represent an expansion of the specimen. Theoretical values of dilatation based on (24) for compression and (26) for extension are 28 cc/cm. and -7.4 cc/cm. respectively. Thus it is seen that the actual dilatations were much smaller than predicted using an ideally plastic model. No allowances have been made for the elastic compression of the specimens, which would probably vary according to the intensity of the hydrostatic pressure, and

would in all cases tend to decrease the dilatation.

The specimens deformed either in thin slip bands, as indicated in Figure 6, or by a general axially symmetric deformation, as in Figure 9. In the case of failure with axial compression, it was usually easy to decide which method of failure had occurred by examining the specimen at the conclusion of a test. In axial extension tests it was much more difficult to decide, a typical specimen being that shown in the photograph (Figure 12). In the case illustrated an axially symmetric neck has formed but there is also some evidence of a shear plane running from top left to bottom right of the sheared zone. In all the extension tests shear was confined to a relatively small zone similar in size to that illustrated in Figure 9b. In compression, however, shearing frequently extended the entire length of the specimen between the plattens. This result is as expected: changes in geometry tend to reduce the critical cross-sections in extension, leading to increased stresses on planes which have slipped, while in compression the cross-section will tend to be increased and slip may well be transferred to a smaller, and hence weaker, plane.

The present series of tests tends to support Habib's conclusion that the effective angle of friction in extension tests may sometimes differ from that in compression. Independent tests by Bishop and Eldin and by Kirkpatrick show that the angle is identical for some sands. A considerably greater volume of experimental evidence is of course needed before any strong assertions can be made. On the evidence to date it does appear, however, that the mechanical behavior of sands may vary in some fundamental manner, governed by such factors as grading, particle shape, porosity, etc. It may be necessary to make many investigations before a clear picture emerges.

Meanwhile it is disturbing to find some sands which do not meet the condition of yield as predicted by plastic theory. In such sands the standard limiting equilibrium approach would not necessarily result in conservative estimates of carrying capacity. Previously, there was a distinct possibility that

all limiting equilibrium states would prove to be equal to or to underestimate the actual carrying capacity, as if the soil were an ideally plastic material.

The need for further investigation is clear. One interpretation of the results of the current series and also of Habib's would be to speculate that the intermediate principal stress adopted a value corresponding to $k = 0.4$ in (8). This estimate is based on the assumptions that the principal stresses remain in the same ratio at all points and that the Coulomb yield criterion applies. Neither assumption has been subjected to any conclusive empirical test, and there seems little doubt that a fuller understanding of the results of the triaxial test must wait upon an independent investigation of the influence on yield of the intermediate principal stress.

Bibliography

1. A. Haar and Th. v. Kármán, Nach. Ges. Wiss. Göttingen, Math.-Phys. Kl., 1909, p. 204.
2. A. W. Bishop and D. J. Henkel, "The Measurement of Soil Properties in the Triaxial Test," Edward Arnold, London, 1957, pp. 190.
3. R. Seiffert, "Untersuchungsmethod um festzustellen ob sich ein gegebenes Baumaterial fur den Bau eines Erddammes eignet," 1er Congrès des Grands Barrages, 1933, Vol. 3, p. 47.
4. T. E. Stanton and F. N. Hveem, "Role of the Laboratory in the Preliminary Investigation and Control of Materials for Low Cost Bituminous Pavements," Proc. XIVth Ann. Mtg. Highway Res. Bd., 1934, Vol. 14 (II), pp. 14-54.
5. L. Rendulic, "Relation between Void Ratio and Effective Principal Stresses for a Remoulded Silty Clay," Proc. 1st Int. Conf. Soil Mech., Foundation Engng., 1936, Vol. 3, pp. 48-53.
6. W. S. Housel, "Internal Stability of Granular Materials," Proc. Am. Soc. Testing Materials, Vol. 36 (II), 1936, pp. 426-468.
7. C. A. Coulomb, "Essai sur une Application des Règles de Maximis et Minimis à quelques Problèmes de Statique Relatif a l'Architecture," Mem. Acad. Sci. (Savants Étrangers), Vol. 7, 1773, p. 343.
8. O. Mohr, "Beiträge zur Theorie des Erddruckes," Z. Arch. u Ing. Ver., Hannover, Vol. 17, 1871, p. 344, Vol. 18, 1872, p. 67, 245.
9. D. C. Drucker, "A More Fundamental Approach to Plastic Stress-Strain Relations," Proc. 1st U.S. Nat. Cong. Applied Mechanics, 1951, pp. 487-491.
10. R. T. Shield, "On Coulomb's Law of Failure in Soils," J. Mech. Phys. Solids, Vol. 4, 1955, pp. 10-16.
11. J. W. Bishop, A. P. Green and R. Hill, "A Note on the Deformable Region in a Rigid-Plastic Body," J. Mech. Phys. Solids, Vol. 4, 1956, p. 256.
12. J. Mandel, "Équilibres par tranches planes des solides," Louis-Jean, Paris, 1942.
13. R. T. Shield, "On Plastic Flow of Metal under Conditions of Axial Symmetry," Proc. Roy. Soc. (U.K.) A, Vol. 233, 1955, pp. 267-286.
14. M. P. Habib, "Nouvelles Recherches en Mécanique du Sol," Annales de L'Institute Technique du Bâtiment et Des Travaux Publics, No. 224, new series, Dec. 1951.
15. M. P. Habib, "Influence of the Variation of the Intermediate Principal Stress on the Shearing Strength of Soils," Proc. 3rd Int. Conf. Soil Mech., Foundation Engng., 1953, Vol. 1, pp. 131-136.
16. A. W. Bishop and A. K. G. Eldin, "The Effect of Stress History on the Relation between ϕ and Porosity in Sand," Proc. 3rd Int. Conf. Soil Mech., Foundation Engng., 1953, Vol. 1, p. 100.

Bibliography (Cont'd)

17. W. M. Kirkpatrick, "The Condition of Failure for Sands," Proc. 4th Int. Conf. Soil Mech., Foundation Engng., 1957, Paper 1b/19, pp. 172-178.
18. R. Hill, "On the State of Stress in a Plastic-Rigid Body at the Yield Point," Phil. Mag., Ser. 7, Vol. 42, 1951, p. 868.
19. R. Hill, J. Mech. Phys. Solids, Vol. 4, 1956, p. 247.

APPENDIX

Uniqueness of applied surface forces when the yield surface is not strictly convex but contains flats.

Theorem** If the prescribed surface velocities acting on a body composed of stable, ideally plastic material are uniform in magnitude and direction, then the component of the resultant surface force in the direction of motion of the surface is uniquely defined.

Proof Consider a body for which the velocities u_i are specified over the region A_u and the tractions T_i are specified over the region A_T of the surface. Suppose a solution with stresses σ_{ij} , strain rates ϵ_{ij} and resultant surface force F_i on A_u . Let σ_{ij}^* , etc., refer to any equilibrium state that does not violate the yield condition and satisfies the traction condition on A_T . By the principle of virtual work

$$\int_{A_u} (T_i - T_i^*) u_i dA = \int_V (\sigma_{ij} - \sigma_{ij}^*) \epsilon_{ij} dV$$

The flow rule for a stable material (see [9]) requires that

$$(\sigma_{ij} - \sigma_{ij}^*) \epsilon_{ij} \geq 0 \quad .$$

When the stress state σ_{ij}^* lies on the same flat on the yield surface as σ_{ij} , the equality holds and

$$\int_{A_u} (T_i - T_i^*) u_i dA = 0 \quad .$$

The velocities u_i are constant in magnitude and direction on A_u , so

$$F_i u_i = F_i^* u_i \quad .$$

Q.E.D.

** This theorem has been proved by Hill [18] for the more restrictive case of a strictly convex yield surface.

Table I

	ϵ_a	:	ϵ_b	:	ϵ_c
A	$(\lambda_1^2 + \lambda_6^2)N^2$:	$-\lambda_1^2$:	$-\lambda_6^2$
AB	$\lambda_1^2 N^2$:	$-\lambda_1^2$:	0
B	$\lambda_1^2 N^2$:	$-(\lambda_1^2 + \lambda_2^2)$:	$\lambda_2^2 N^2$
BC	0	:	$-\lambda_2^2$:	$\lambda_2^2 N^2$
C	$-\lambda_3^2$:	$-\lambda_2^2$:	$(\lambda_2^2 + \lambda_3^2)N^2$
CD	$-\lambda_3^2$:	0	:	$\lambda_3^2 N^2$
D	$-(\lambda_3^2 + \lambda_4^2)$:	$\lambda_4^2 N^2$:	$\lambda_3^2 N^2$
DE	$-\lambda_4^2$:	$\lambda_4^2 N^2$:	0
E	$-\lambda_4^2$:	$(\lambda_4^2 + \lambda_5^2)N^2$:	$-\lambda_5^2$
EF	0	:	$\lambda_5^2 N^2$:	$-\lambda_5^2$
F	$\lambda_6^2 N^2$:	$\lambda_5^2 N^2$:	$-(\lambda_5^2 + \lambda_6^2)$
FA	$\lambda_6^2 N^2$:	0	:	$-\lambda_6^2$

$\lambda_1 \dots \lambda_6$ are constants; $N = \tan\left(\frac{\pi}{4} + \frac{\phi}{2}\right)$

Table II

	Initial Porosity	Lateral Pressure p	Mean Axial Pressure \bar{q}	Dilatation Rate
Test	%	kg/cm ²	kg/cm ²	cc/cm
A1	49	0.6	2.4	4.9
A2	49	0.7	2.7	3.7
A3	51	1.0	3.7	2.6
A4	47	1.4	5.4	2.7
A5	51	1.6	6.0	2.0
A6	-	2.1	8.4	-
A7	49	2.6	10.6	2.2
A8	51	2.6	9.6	1.2
A9	49	2.6	9.8	1.6
A10	50	2.8	10.7	2.3
A11	49	2.8	10.5	-
A12	50	3.0	11.5	1.8
B1	51	0.6	2.4	5.3
B2	50	1.2	4.4	4.7
B3	49	1.8	7.0	-
B4	50	2.4	8.4	1.8
C1	49	1.0	0.3	-1.4
C2	50	2.0	0.6	-
C3	51	3.0	1.2	0
C4	50	4.0	1.3	0
C5	48	5.0	2.1	0
D1	51	1.6	0.6	-0.3
D2	50	3.2	1.2	0
D3	50	3.7	1.2	-0.1
D4	50	4.7	1.6	0
D5	51	5.6	2.1	-
D6	52	6.4	2.4	+0.3

Table II Results of triaxial tests on crushed quartz (Lantern Hill)

Compression tests

Series A - failure by increasing axial pressure

Series B - failure by decreasing lateral pressure

Extension tests

Series C - failure by decreasing axial pressure

Series D - failure by decreasing lateral pressure

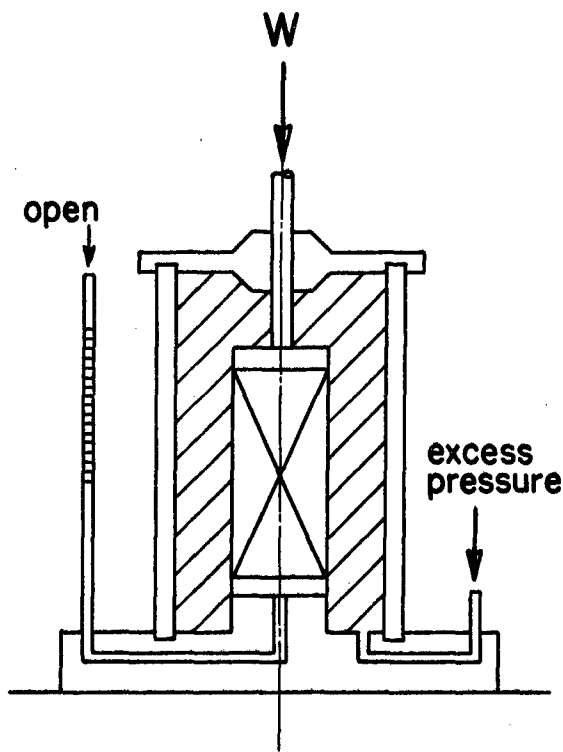


FIG. 1

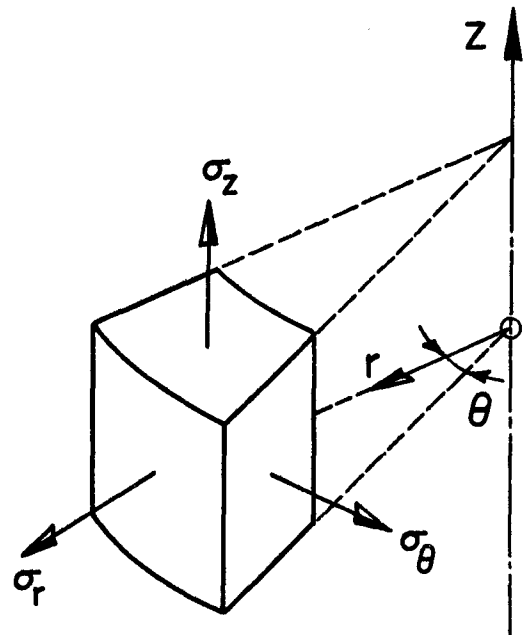


FIG. 2

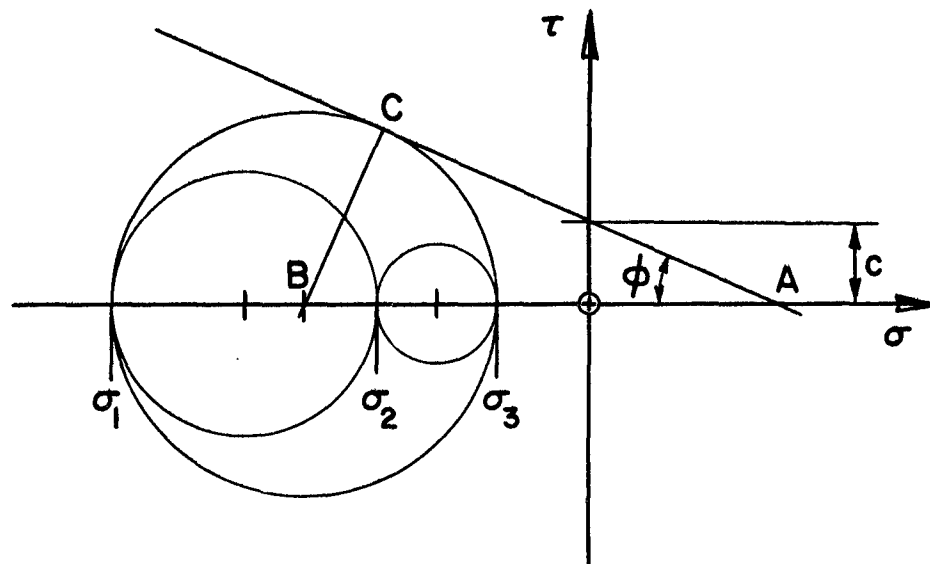


FIG. 3

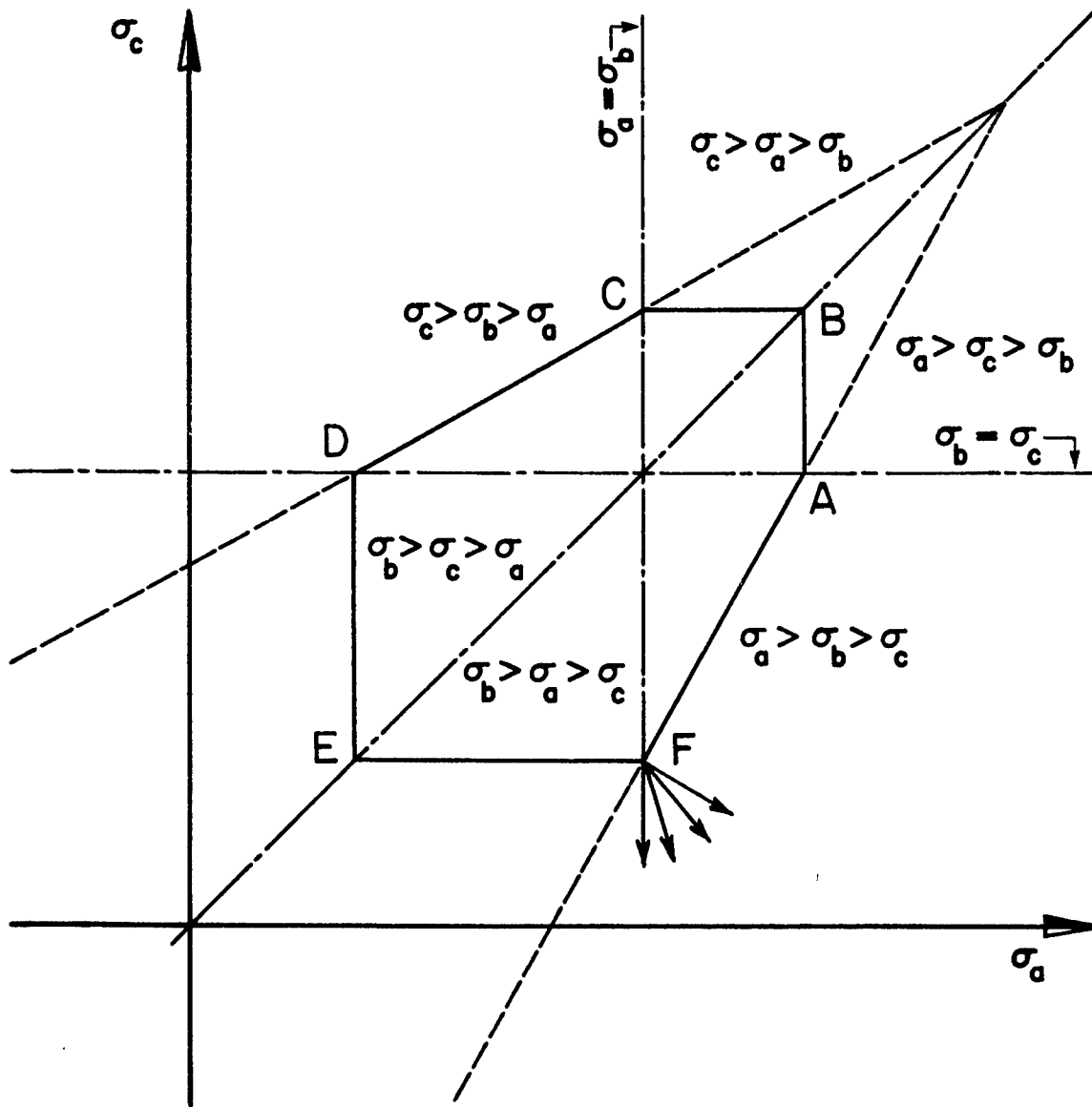


FIG. 4

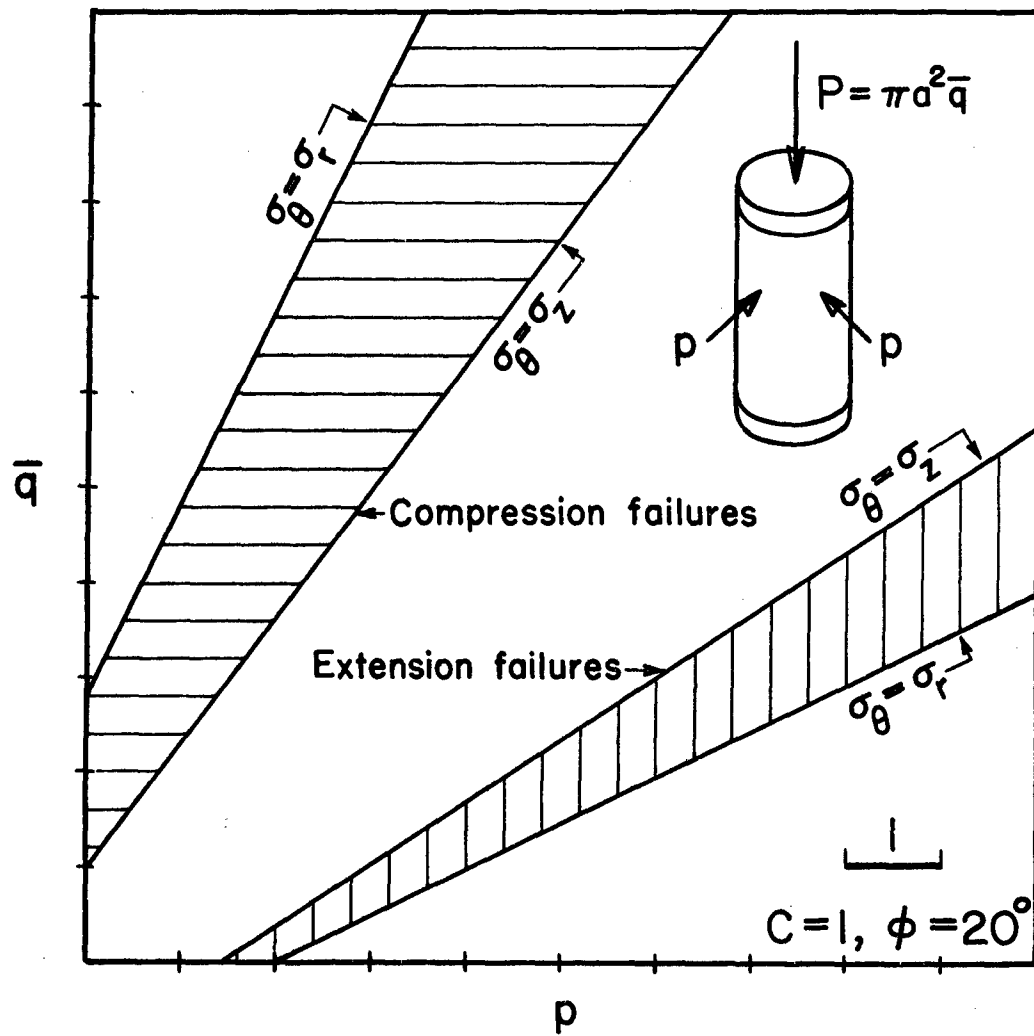


FIG. 5

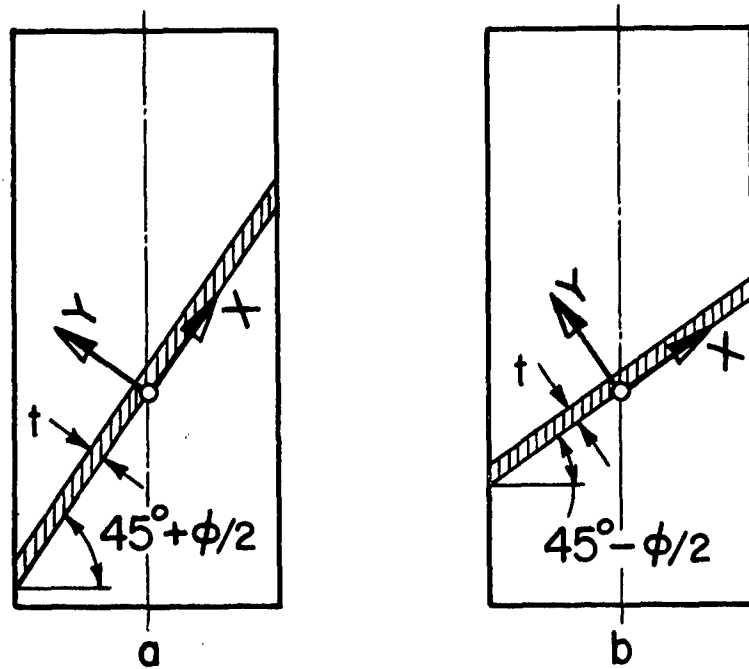


FIG. 6 Possible slip planes for: a) Compression failures
b) Extension failures

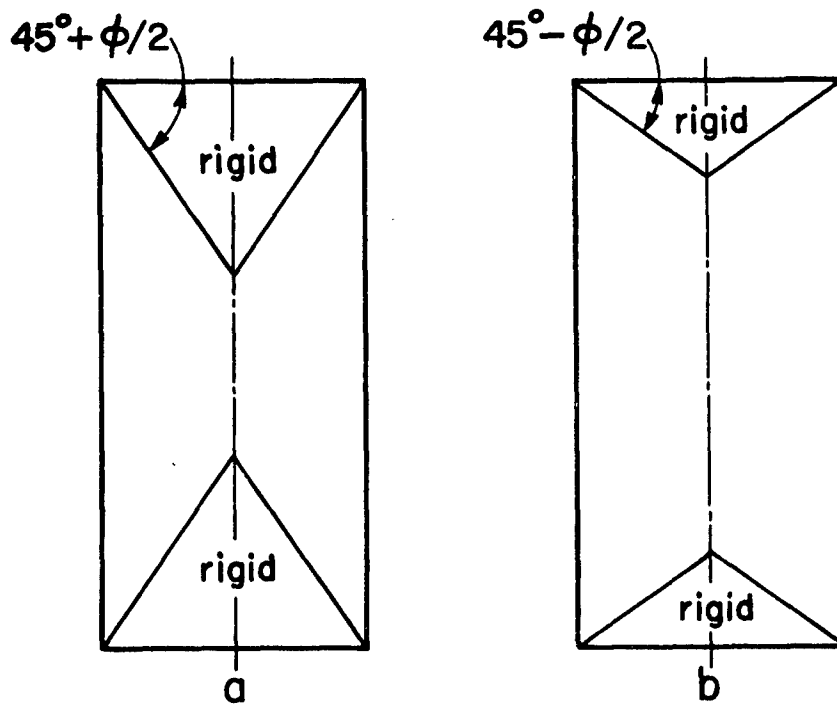


FIG. 7 Extent of the deformable region for: a) Compression failures
b) Extension failures

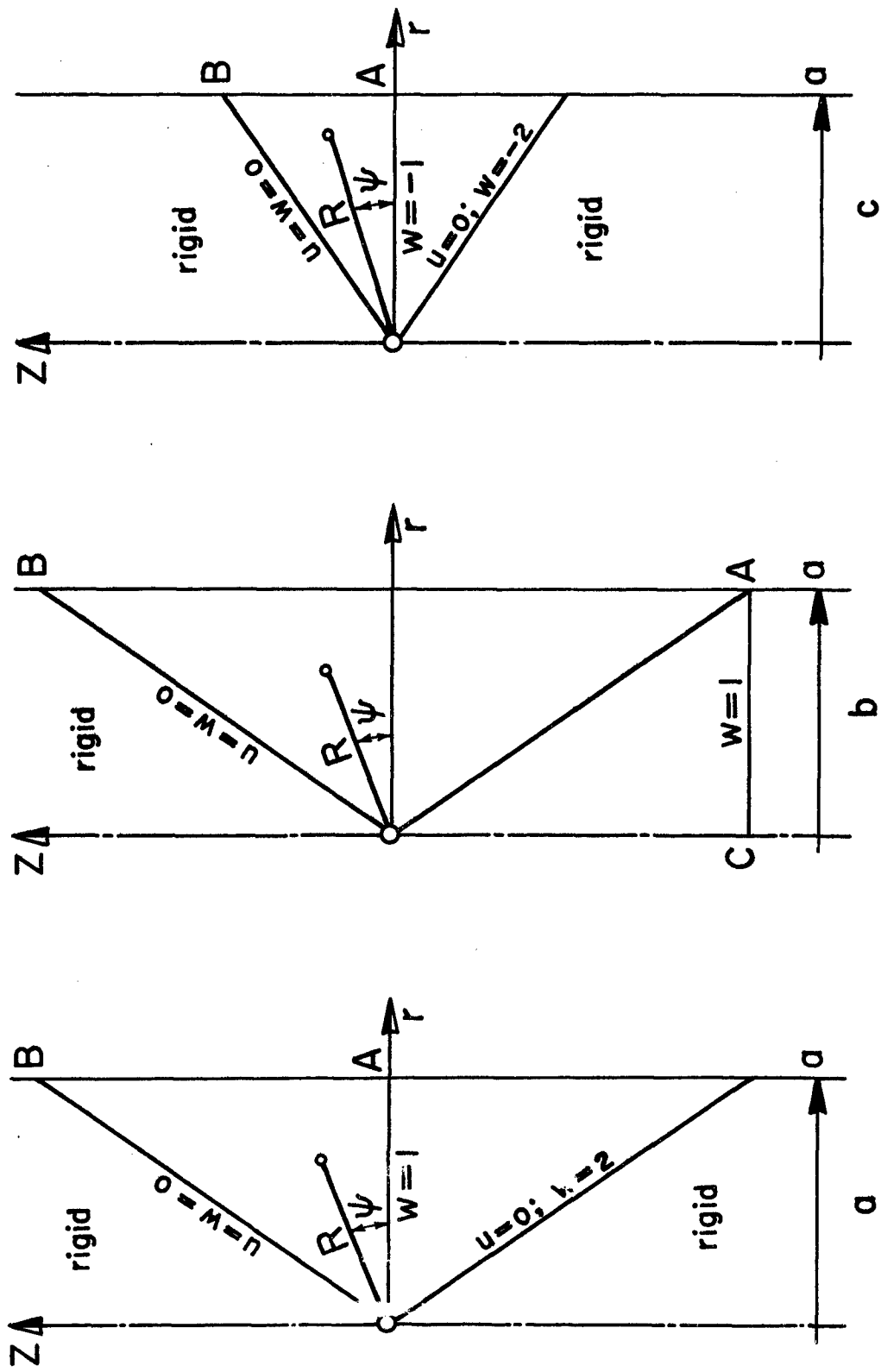
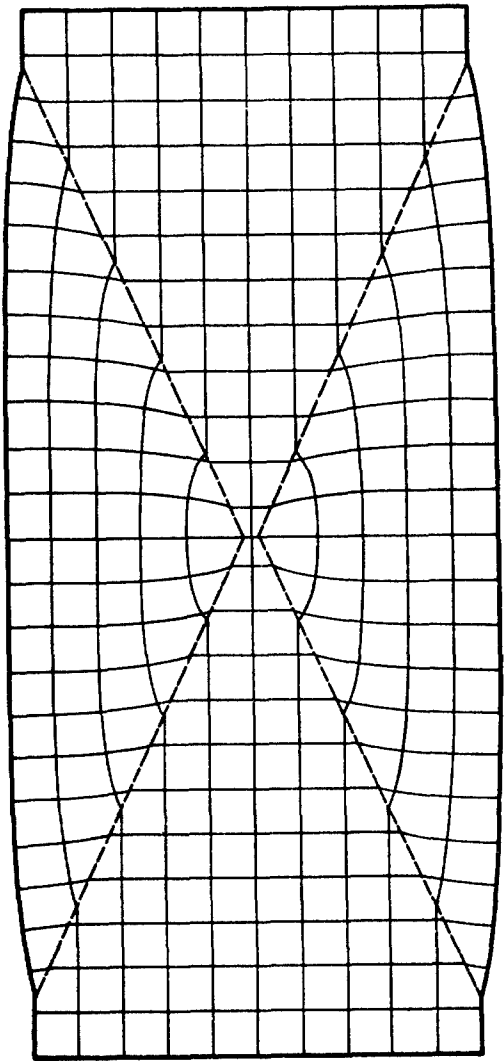
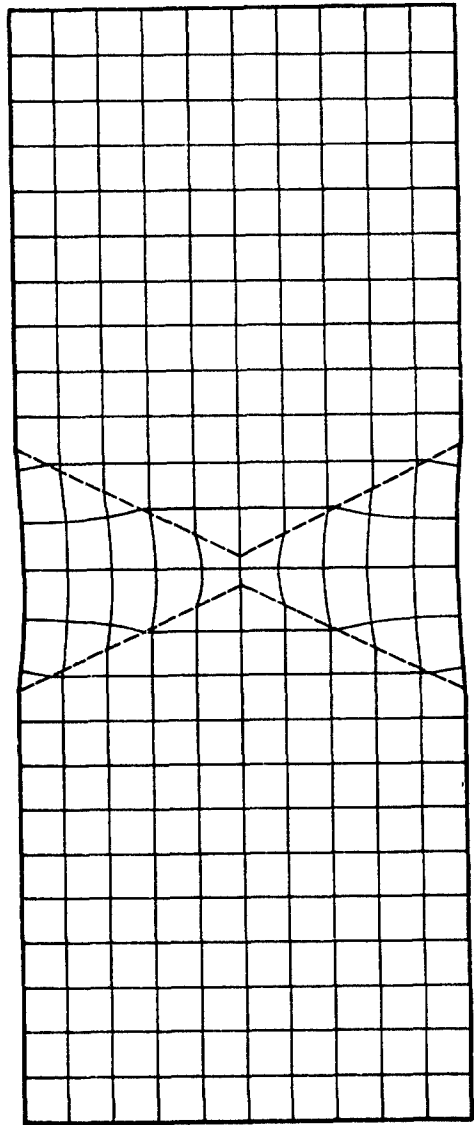


FIG.8 Regions of deformation with axial symmetry: aab) are for failure with axial compression and c) for failure with axial extension



a



b

FIG. 9

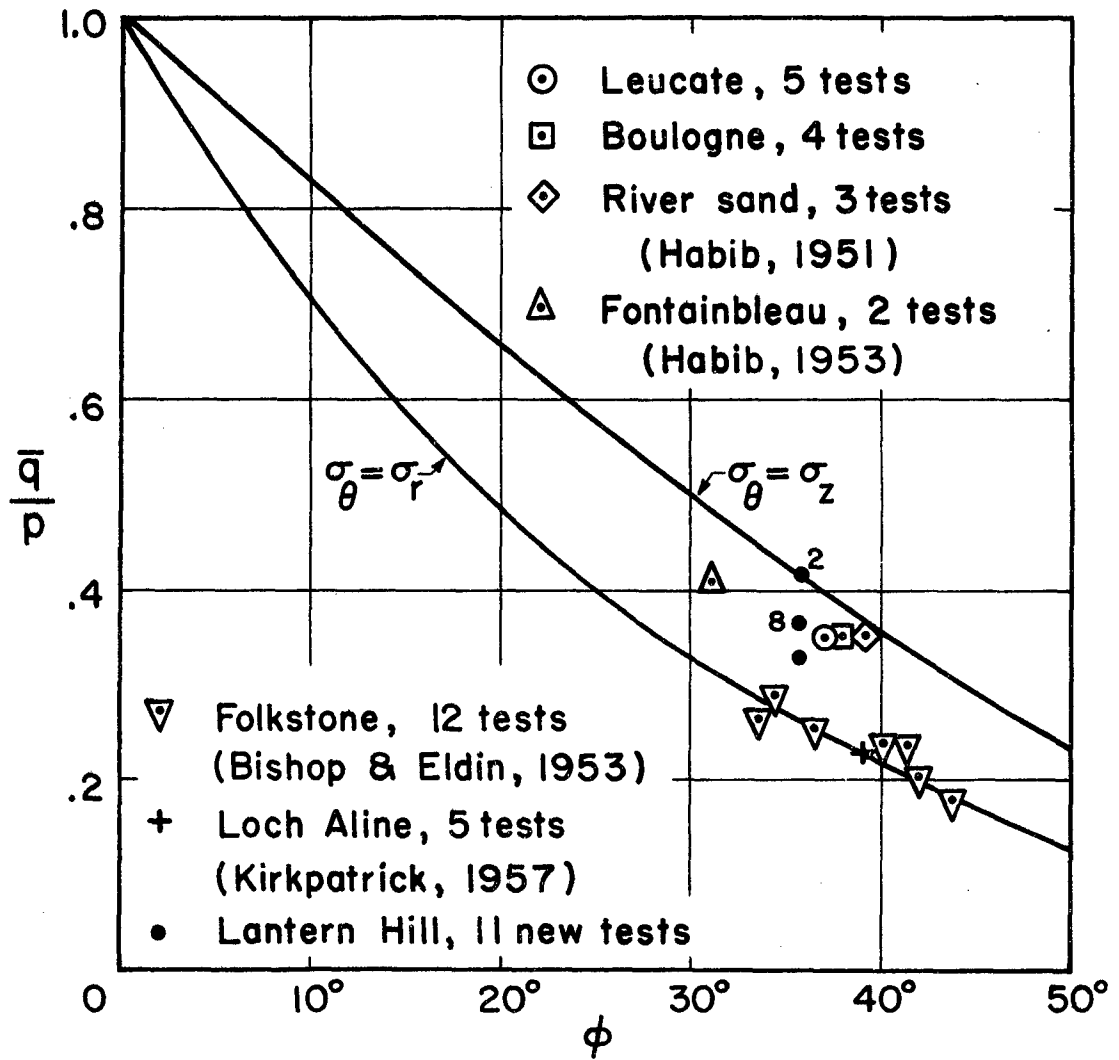


FIG. 10 Triaxial extension tests on sand. Ratio of axial to lateral pressure vs. angle of friction computed from compression tests.

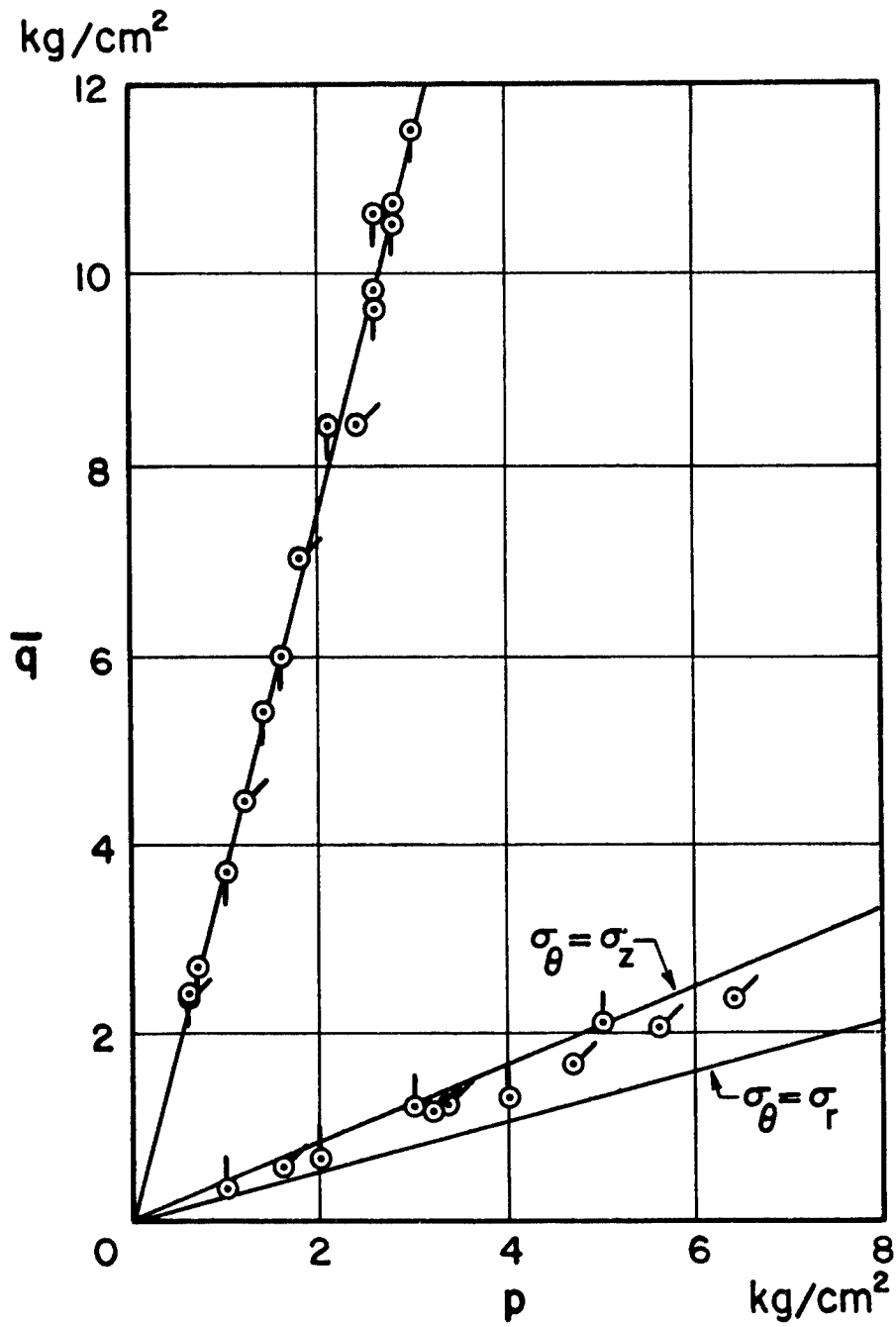


FIG. 11 Triaxial tests on crushed quartz sand (Lantern Hill)

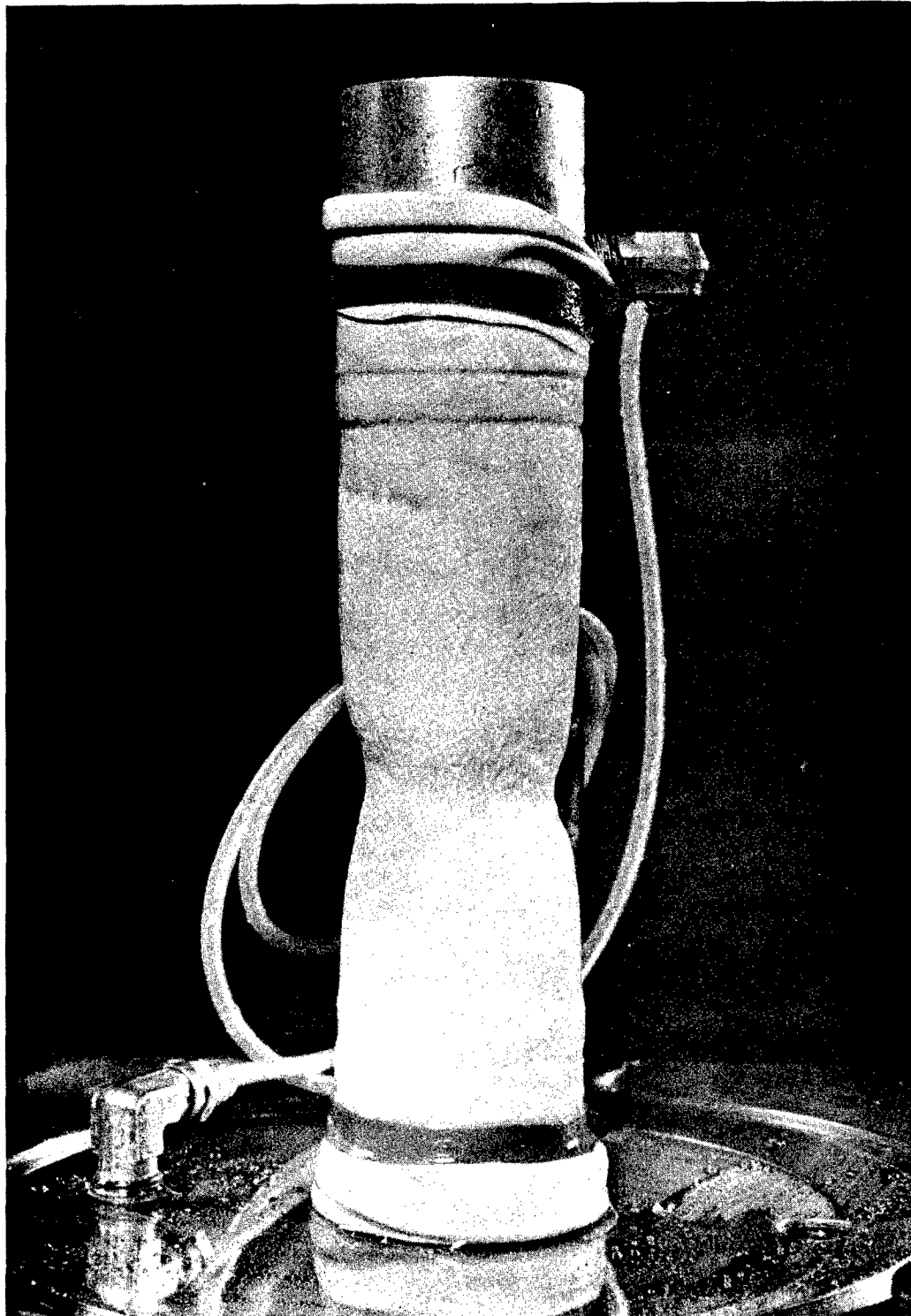


FIG.12 Appearance of a specimen after an extension failure, showing the limited extent of the deformed zone. (see: FIG. 9b)

DISTRIBUTION LIST

Commanding General Aberdeen Proving Gd., Md. ATTN: ORDBG-DPS ATTN: Tech Library	3 2	United States Navy Industrial College of the Armed Forces Washington, D. C. ATTN: Vice Deputy Commandant	1
Commandant Ordnance School Aberdeen Proving Gd., Md.	1	Dept. of National Defense Dr. N. W. Morton Scientific Advisor Chief of General Staff Army Headquarters Ottawa, Ontario, Canada	1
Director Air University Library Maxwell AFB, Alabama ATTN: AUL-8329	1	Chief of Ordnance Department of the Army Washington 25, D. C. ATTN: ORDTB	2
British Joint Service Mission Ministry of Supply P. O. Box 680 Benjamin Franklin Station Washington, D. C. ATTN: Reports Officer	2	Commanding Officer Office of Ordnance Research Box CM, Duke Station Durham, North Carolina	3
British Joint Service Mission Ministry of Supply Staff 1800 K Street N. W. Washington, D. C.	6	Chief Office of Naval Research Washington, D. C.	1
Canadian Army Staff 2450 Massachusetts Avenue Washington, D. C.	4	Headquarters Ordnance Weapons Command Research & Development Division ORDOW-TB Rock Island, Illinois	2
Director Waterways Experiment Station Vicksburg, Mississippi	3	Commanding Officer Transportation Research & Development Command Fort Eustis, Virginia ATTN: Special Projects Div.	2
Unit X Documents Expediting Project Library of Congress Washington, D. C. Stop 303	1	Army Research Office Arlington Hall Station Arlington 12, Virginia	1
Exchange and Gift Division Library of Congress Washington 25, D. C.	1	Commander Armed Services Technical Information Agency Arlington Hall Station Arlington 12, Virginia	1
Detroit Arsenal AFF Liaison Office, CONARC Center Line, Michigan	12	Commanding Officer Diamond Ordnance Fuze Laboratories Washington 25, D. C. ATTN: ORDTL 012	1
Detroit Arsenal Canadian Liaison Office Center Line, Michigan	4		
Detroit Arsenal Technical Library Center Line, Michigan	2		

DISTRIBUTION LIST (Continued)

Superintendent U. S. Military Academy West Point, New York ATTN: Prof of Ordnance	1	Midwest Applied Science Corp. Lafayette Load & Trust Bldg. Lafayette, Indiana ATTN: Dr. J. L. Bogdanoff	1
Superintendent U. S. Naval Academy Annapolis, Md.	1	Colleges and Universities	100
Professor F. J. Converse Professor of Soil Mechanics California Inst. of Technology Pasadena 4, California	1		
Professor D. C. Drucker Brown University Providence 12, Rhode Island	1		
Dr. F. E. Brubbs Ch, Weapons Systems Lab. Ballistic Research Lab. Aberdeen Proving Gd., Md.	1		
Mr. W. T. Milliken, Jr. Cornell Aeronautical Lab., Inc. Cornell University Buffalo 21, New York	1		
Dr. Peter Kyropoulos Exec. in Charge Tech. Div. General Motors Styling Technical Center Warren, Michigan	1		
Professor E. T. Vincent Dept. of Mechanical Engr. University of Michigan Ann Arbor, Michigan	1		
Mr. E. T. Norelius, Chairman SAE Off-Highway Vehicle Mobility Advisory Committee 5152 Hampshire Drive Minneapolis, Minnesota	14		
Wilson, Nuttall and Raimond Engineers Inc. Chestertown, Maryland	1		
Southwest Research Institute 8500 Culebra Road San Antonio 6, Texas	1		
Planning Research Corporation Los Angeles, California	1		